The reweighted path ensemble

Rogal, J.; Lechner, W.; Juraszek, J.; Ensing, B.; Bolhuis, P.G.

DOI
10.1063/1.3491817
Publication date
2010
Document Version
Final published version
Published in
Journal of Chemical Physics

The reweighted path ensemble

Jutta Rogal,[1] Wolfgang Lechner,[2] Jarek Juraszek,[3] Bernd Ensing,[2] and Peter G. Bolhuis[2,a)]
[1]*Interdisciplinary Centre for Advanced Materials Simulation (ICAMS), Ruhr University Bochum, 44780 Bochum, Germany*
[2]*van't Hoff Institute for Molecular Sciences, University of Amsterdam, Nieuwe Achtergracht 166, Amsterdam 1018WV, The Netherlands*
[3]*Spanish National Cancer Research Centre (CNIO), Melchor Fernandez Almagro 3, Madrid 28029, Spain*

(Received 29 April 2010; accepted 20 August 2010; published online 1 November 2010)

We introduce a reweighting scheme for the path ensembles in the transition interface sampling framework. The reweighting allows for the analysis of free energy landscapes and committor projections in any collective variable space. We illustrate the reweighting scheme on a two dimensional potential with a nonlinear reaction coordinate and on a more realistic simulation of the Trp-cage folding process. We suggest that the reweighted path ensemble can be used to optimize possible nonlinear reaction coordinates. © *2010 American Institute of Physics*.
[doi:10.1063/1.3491817]

I. INTRODUCTION

Rare events in complex high dimensional systems, such as crystal nucleation, protein folding, and chemical reactions in solution, remain a challenge for computational studies, because a naive straightforward sampling of the phase space by employing molecular simulation hardly ever samples the important barrier regions. Over the years many approaches have been developed to address the rare event sampling problem. Among them are umbrella sampling,[1] flooding,[2] metadynamics,[3] and many others.[4] These methods produce a free energy profile or landscape in terms of an *a priori* defined reaction coordinate variable. Application of, for instance, the transition state theory based reactive flux method,[5,6] hyperdynamics,[7,8] temperature accelerated dynamics,[9] or parallel replica[10] can also yield the dynamical evolution of a system, including the phenomenological rate constants. However, while for simple systems constructing a reaction coordinate can be easy, for complex systems a description of such a coordinate is usually not trivial. A poorly chosen collective variable might result in a wrong estimate for the transition state, in a statistically unmeasurable transmission coefficient due to recrossings, and in mechanisms that are even qualitatively completely wrong.[11] A prime example of a complex process for which a suitable reaction coordinate is almost impossible to guess intuitively is protein folding.

One possible solution to this problem is the application of the transition path sampling method (TPS), designed to harvest a collection of dynamical pathways between a predefined initial and final state.[11,12] The major advantage of this method is that the reaction coordinate for the transition between the initial and final state is not assumed. Moreover, as the dynamics used in TPS is the actual underlying physical dynamics, the method samples the true kinetic mechanism. The outcome of a TPS simulation is an ensemble of pathways that can be analyzed to extract qualitative information on the mechanism and the reaction coordinate. In addition, the TPS method yields the rate constant by computing the reversible work to constrain the path ensemble to the final state. Transition interface sampling (TIS) is a TPS version that improves on this rate constant calculation by introducing a number of interfaces, through which the positive effective flux can be measured.[13] The TIS expressions for the rate constant form the basis of the forward flux sampling (FFS), which was especially developed for nonequilibrium dynamics, but also holds for equilibrium systems.[14] TIS can be used to obtain the rate constant and the free energy profile as a function of a progress parameter, simultaneously.[15] The main result following from TIS is the crossing probability histograms as a function of the progress parameter, which can be joined together by the weighted histogram analysis method (WHAM).[16] Recent work showed that combining TIS with the replica exchange formalism (RETIS) improves the efficiency of the path sampling significantly.[17,18]

The above path sampling methods make use of reweighting of histograms as a function of a certain collective variable. In this work we show that the path ensemble *itself* can be reweighted using the TIS crossing probabilities. This reweighting results in a path ensemble where each path has a weight that represents the probability of occurring in an unbiased path ensemble. It is thus a correction for the bias that the TIS approach introduces for each interface. The path weight implies that each time slice in the path also has the same weight. The general idea of combining multiple path ensembles was independently put forward in a recent paper by Minh and Chodera.[19]

As the reweighted path ensemble (RPE) is an approximation of unbiased trajectories, we can use it not only to compute the free energy as a function of the reaction coordinate, but as a function of *any* coordinate. Moreover, because we know where each path ends, we can project the committor as a function of any coordinate. In addition, as will be discussed at length in Ref. 20, this allows for extract-

a)Electronic mail: p.g.bolhuis@uva.nl.

ing information from the RPE for an analysis of nonlinear reaction coordinates, including parts of the mechanism that are far away from the transition state region.

The remainder of paper is organized as follows. First, we introduce the path ensembles and the reweighting scheme in Sec. II. We illustrate the reweighting method on a simple two–dimensional (2D) potential. In addition, we apply it to a more realistic system, the Trp-cage folding transition, which we studied in atomistic detail in a previous paper.[21,22] We end with concluding remarks.

II. METHODS

A. The path ensembles

A trajectory (or path) is defined as $\mathbf{x}^L \equiv \{\mathbf{x}_0, \mathbf{x}_1, \cdots \mathbf{x}_L\}$, a sequence of phase space points $\mathbf{x}=\{\mathbf{r}^N, \mathbf{p}^N\}$, where $\mathbf{r}$ and $\mathbf{p}$ denote the coordinates and momenta of the N-particle system. The time step between these sequential points, or time slices, is Δt, resulting in a total time duration of the path $\mathcal{T}=L\Delta t$. The probability of finding a certain trajectory $\mathbf{x}^L$ is proportional to[12]

$$\pi[\mathbf{x}^L] = \rho(\mathbf{x}_0)\prod_{i=0}^{L-1} p(\mathbf{x}_i \to \mathbf{x}_{i+1}), \tag{1}$$

where $\rho(\mathbf{x})$ denotes the steady state distribution, e.g., the canonical distribution, and $p(\mathbf{x}\to\mathbf{y})$ represents the Markovian probability to go from a state $\mathbf{x}$ to $\mathbf{y}$ within one time interval.[23] The normalized path probability is

$$\mathcal{P}[\mathbf{x}^L] = \pi[\mathbf{x}^L]/Z. \tag{2}$$

Z is normalization factor that is akin to a partition function and is given by

$$Z \equiv \int \mathcal{D}\mathbf{x}^L \pi[\mathbf{x}^L], \tag{3}$$

where the integration runs over all possible paths of all lengths.

A path sampling of rare events only should sample paths that lead over the barrier from an initial stable state A to a final stable state B. This can be achieved by putting a constraint in the path distribution of Eq. (2), such that only paths that connect A to B contribute to the distribution. This transition path ensemble is

$$\mathcal{P}_{AB}[\mathbf{x}^L] = h[\mathbf{x}^L]\pi[\mathbf{x}^L]/Z_{AB}, \tag{4}$$

with again Z_{AB} a normalizing factor defined by $\int \mathcal{D}\mathbf{x}^L \mathcal{P}_{AB}[\mathbf{x}^L]=1$. The indicator function $h[\mathbf{x}^L]$ is defined as

$$h[\mathbf{x}^L] = \begin{cases} 1 & \text{if} \quad \mathbf{x}_0 \in A \wedge \mathbf{x}_L \in B \wedge \\ & \forall\{j|0<j<L\}:\mathbf{x}_j \notin (A \cup B) \\ 0 & \text{otherwise}, \end{cases} \tag{5}$$

such that sampling this distribution only selects paths that just leave A and just enter B.

TIS (Ref. 13) introduces $n+1$ nonintersecting interfaces between A and B described by a progress parameter $\lambda(\mathbf{x})$ which is a function of the phase point $\mathbf{x}$. The $n+1$ interfaces are defined by the ordered sequence $\lambda_0, \lambda_1, \ldots, \lambda_n$, where the first interface λ_0 equals the boundary of state A, and the last one λ_n is identical to the boundary of state B. The TIS path ensemble that we define here selects paths that start in A, and either end in B or return to A, provided that they have crossed a certain interface λ_i. Defining the region of phase space beyond interface i by $\Lambda_i^+ = \{\mathbf{x}:\lambda(\mathbf{x}) > \lambda_i\}$, the path probability is

$$\mathcal{P}_{A\Lambda_i}[\mathbf{x}^L] = \tilde{h}_i^A[\mathbf{x}^L]\pi[\mathbf{x}^L]/Z_{A\Lambda_i}, \tag{6}$$

where the normalizing factor $Z_{A\Lambda_i}$ is again defined by $\int \mathcal{D}\mathbf{x}^L \mathcal{P}_{A\Lambda_i}[\mathbf{x}^L]=1$. The indicator function for paths that begin in A, end in A or B, and cross λ_i is

$$\tilde{h}_i^A[\mathbf{x}^L] = \begin{cases} 1 & \text{if} \quad \mathbf{x}_0 \in A \wedge \mathbf{x}_L \in (A \cup B) \wedge \\ & \forall\{j|0<j<L\}:\mathbf{x}_j \notin (A \cup B) \wedge \\ & \exists\{j|0<j<L\}:\mathbf{x}_j \in \Lambda_i^+ \\ 0 & \text{otherwise}. \end{cases} \tag{7}$$

The TIS path ensemble can be sampled using the regular shooting algorithm.[13] Employing a combination of the replica exchange formalism with the TIS algorithm (RETIS) improves the sampling efficiency.[17,18] From the TIS path ensemble of interface i one can extract the crossing probability $P(\lambda|\lambda_i)$ for each value of λ for the interval $\lambda_i < \lambda < \lambda_B$ from the histogram

$$P_A(\lambda|\lambda_i) = \int \mathcal{D}\mathbf{x}\mathcal{P}_{A\Lambda_i}[\mathbf{x}^L]\theta(\lambda_{\max}[\mathbf{x}^L] - \lambda), \tag{8}$$

with $\lambda_{\max}[\mathbf{x}^L]$ the maximum value of λ reached for each trajectory $\mathbf{x}^L$ in the path ensemble $A\Lambda_i$ and $\theta(x)$ is the Heaviside step function. For all values $\lambda > \lambda_i$ the crossing probability histograms of different interfaces $j \geq i$ in Eq. (8) differ only by a multiplicative factor. Therefore, all interface histograms can be joined together using the weighted histogram analysis method (WHAM).[16] In the appendix we show that the total histogram can be expressed as

$$P_A(\lambda|\lambda_1) = \sum_{i=1}^{n-1} \bar{w}_i^A \theta(\lambda_{i+1} - \lambda)\,\theta(\lambda - \lambda_i) \sum_{j=1}^{i} P_A(\lambda|\lambda_j), \tag{9}$$

where the weights $\bar{w}_i^A$ are obtained by applying WHAM. For TIS, the weights are given by $\bar{w}_i^A = (\Sigma_{i=1}^{n-1} Z_A / Z_{A\Lambda_i})^{-1}$.

The rate constant $k_{AB} = \phi_{01} P(\lambda_n|\lambda_1)$ follows from the product of the crossing probability $P(\lambda_n|\lambda_1)$ and the flux ϕ_{01} through interface λ_1. For the reverse process $B \to A$ corresponding expressions can be formulated (see appendices). Free energy profiles as a function of λ follow from projections of the forward and reverse path ensembles, while carefully avoiding overcounting.[15,18]

B. The reweighted path ensemble

The unbiased path ensemble (Fig. 1) for A is given by all paths that leave A and end in A or in B. The corresponding path probability is

$$\mathcal{P}_A[\mathbf{x}^L] = h_A(\mathbf{x}_0)\pi[\mathbf{x}^L]/Z_A, \tag{10}$$

where the indicator function $h_A(\mathbf{x})=1$ for points $\mathbf{x} \in A$ and zero otherwise, and $Z_A \equiv \int \mathcal{D}\mathbf{x} h_A(\mathbf{x}_0)\pi[\mathbf{x}^L]$. These paths are depicted in Fig. 1 as red solid trajectories outside of A. The

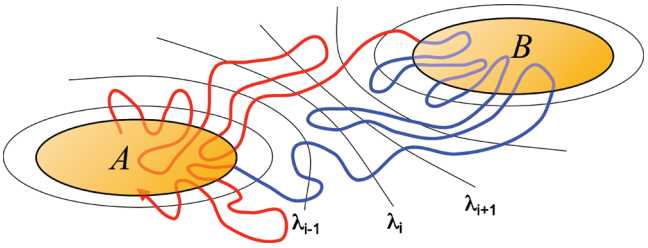

FIG. 1. Cartoon of the unbiased path ensemble in the context of TIS. The red and blue curves outside the (shaded) stable state regions denote the unbiased path ensemble for A and B, respectively.

counterpart, the unbiased path ensemble for state B, can be defined similarly and is given as blue lines outside of B. If one could sample this ensemble directly then all properties of the rare event of interest could be directly computed. In particular, the unbiased path ensemble allows for extracting rate constants, free energies, and a reaction coordinate. However, sampling this ensemble is the very problem we would like to solve in the first place.

Nevertheless, just as the WHAM method can reweight the crossing probabilities, it can reweight the TIS path ensembles using

$$\mathcal{P}_A[\mathbf{x}^L] = \sum_{j=1}^{n-1} \mathcal{P}_{A\Lambda_i}[\mathbf{x}^L] W^A[\mathbf{x}^L], \tag{11}$$

where each path is given a certain weight $W^A[\mathbf{x}^L] \equiv \Sigma_{i=1}^{n-1} \bar{w}_i^A g_i^A[\mathbf{x}^L]$. Similar to the theta functions in Eq. (9), the function $g_i^A[\mathbf{x}^L] = \theta(\lambda_{\max}[\mathbf{x}^L] - \lambda_i)\theta(\lambda_{i+1} - \lambda_{\max}[\mathbf{x}^L])$ selects the correct weight $\bar{w}_i^A$ for a path that has its the maximum λ between interface i and $i+1$. To be meaningful, the reweighted path ensemble Eq. (11) has to be equivalent to Eq. (10). In Appendix A we show that for this condition to hold, the weights $\bar{w}_i^A$ for this path ensemble are identical to those for the crossing histograms [cf. Eq. (9)]. Thus, the weights obtained by matching the crossing histograms with WHAM give access to the unbiased path ensemble from state A.

By defining a similar expression for the reverse process the joint path ensemble for the forward and reverse process is

$$\mathcal{P}[\mathbf{x}^L] = c_A \sum_{j=1}^{n-1} \mathcal{P}_{A\Lambda_j}[\mathbf{x}^L] W^A[\mathbf{x}^L] + c_B \sum_{j=1}^{n-1} \mathcal{P}_{B\Lambda_j}[\mathbf{x}^L] W^B[\mathbf{x}^L]. \tag{12}$$

The unknown constants c_A and c_B follow from matching the AB and BA histograms, as explained in the appendices.

This reweighted path ensemble only takes into account paths that leave A (or B) and cross an interface, not the paths that remain in A (or B) and do not cross any interfaces. However, these paths are easily accessible from the flux computation, or from the additional first and last interface ensemble $P_{\Lambda_1}^-$ (and $P_{\Lambda_{n-1}}^+$) in the RETIS framework.[17,18] The complete path ensemble is then found by adding $P_{\Lambda_1}^-$ and $P_{\Lambda_{n-1}}^+$ to Eq. (12), where the final and initial parts of the trajectories in $P_{\Lambda_1}^-$ between λ_0 and λ_1 and likewise in $P_{\Lambda_{n-1}}^+$ between λ_n and λ_{n-1} are removed to avoid double counting. (Note that in many applications $\lambda_0 = \lambda_1$, although this is not required.) The complete reweighted path ensemble finally becomes

$$\mathcal{P}_c[\mathbf{x}^L] = c_A \left[w_1^A P_{\Lambda_1}^- + \sum_{j=1}^{n-1} \mathcal{P}_{A\Lambda_j}[\mathbf{x}^L] W^A[\mathbf{x}^L] \right] + c_B \left[w_{n-1}^B P_{\Lambda_{n-1}}^+ + \sum_{j=1}^{n-1} \mathcal{P}_{B\Lambda_j}[\mathbf{x}^L] W^B[\mathbf{x}^L] \right]. \tag{13}$$

In summary, the idea of the RPE is to obtain the unbiased path ensemble. While paths crossing the barrier are very rare, they are sampled through TIS and obtain their corrected weight through applying WHAM. The statistics of the ensemble is correct and follows that of Eq. (10).

C. Projection of the free energy and committor surfaces

The RPE can be used to project the free energy on an arbitrary m-dimensional collective variable space $\boldsymbol{q} = \{q^{(1)}, q^{(2)}, \ldots, q^{(m)}\}$. The free energy follows from the probability $p(\boldsymbol{q})$ to find a configuration in the unbiased ensemble at a certain point $\boldsymbol{q}$

$$F(\boldsymbol{q}) = -k_B T \ln p(\boldsymbol{q}) + \text{const.}, \tag{14}$$

where k_B is Boltzmann's constant. This probability is given by

$$p(\boldsymbol{q}) = C \int \mathcal{D}\mathbf{x}^L \sum_{k=0}^{L} \prod_{i=1}^{m} \delta(q^{(i)}(\mathbf{x}_k) - q^{(i)}) \mathcal{P}_c[\mathbf{x}^L], \tag{15}$$

where $\delta(x)$ is the Dirac delta function and C a normalizing constant. Besides the free energy we can project the averaged $\bar{p}_B$ committor function on arbitrary surfaces, by using the indicator function $h_B(\mathbf{x}_L)$,

$$\bar{p}_B(\boldsymbol{q}) = \frac{\int \mathcal{D}\mathbf{x}^L \Sigma_{k=0}^{L} \Pi_{i=1}^{m} \delta(q^{(i)}(\mathbf{x}_k) - q^{(i)}) \mathcal{P}_c[\mathbf{x}^L] h_B(\mathbf{x}_L)}{\int \mathcal{D}\mathbf{x}^L \Sigma_{k=0}^{L} \Pi_{i}^{m} \delta(q^{(i)}(\mathbf{x}_k) - q^{(i)}) \mathcal{P}_c[\mathbf{x}^L]}, \tag{16}$$

where $h_B(\mathbf{x}) = 1$ if $x \in B$ and zero otherwise. This expression holds because each slice on the path can be seen as a realization of a committor shot. It is important to realize that $\bar{p}_B(\boldsymbol{q})$ is an *averaged* committor and not the full committor $p_B(\boldsymbol{r})$. The difference is that the full committor gives a distribution that can be used for a committor test (see, e.g., Ref. 24), whereas $\bar{p}_B(\boldsymbol{q})$ is only the average. While, in principle, the RPE contains also the full committor, in practice we do not have access to $p_B(\boldsymbol{r})$ because there is usually only one shot for each $\boldsymbol{r}$, thus only a 0 or a 1. Nevertheless, $\bar{p}_B$ can yield crucial hints for reaction coordinate analysis.[25,26] In principle, one can project any other property of the path ensemble in this way.

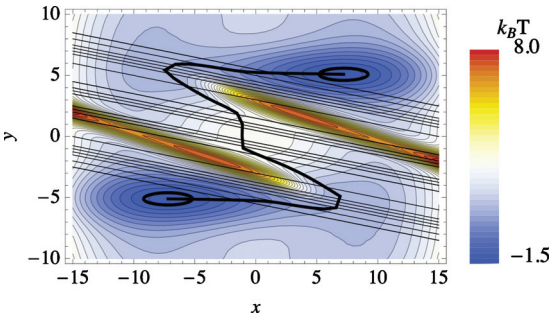

FIG. 2. The z-potential as a function of x and y. The stable states are indicated by ellipses. The location of the 28 linear interfaces is described by $y=-0.2x+\lambda$. The values for λ are given in the main text. The minimum energy pathway is depicted as well.

III. RESULTS AND DISCUSSION

A. The *z*-potential

1. The potential

In this section we employ a two dimensional model system for which the potential is given by

$$V(x,y) = \frac{x^4+y^4}{20\,480} - 3e^{-0.01(x+5)^2-0.2(y+5)^2} - 3e^{-0.01(x-5)^2-0.2(y-5)^2} + \frac{5e^{-0.2(x+3(y-3))^2}}{1+e^{-x-3}} + \frac{5e^{-0.2(x+3(y+3))^2}}{1+e^{x-3}} + 3e^{-0.01(x^2+y^2)}. \quad (17)$$

This potential is visualized in Fig. 2. It has two stable states, one at $(-7.2,-5.1)$ labeled A and one at $(7.2,5.1)$ labeled B. These two minima are separated by a barrier in the shape of the letter s (or a reversed z), due to the presence of two high potential ridges. The potential at the origin is $V=4.28k_BT$ above the minima. The minimum energy pathway is indicated and roughly follows the s-shape.

The system consist of a single particle evolving according to Langevin dynamics on this potential. For details on the algorithm see, e.g., Ref. 12. The friction is set to $\gamma=1$, the temperature is set to $\beta=4$, where $\beta=1/k_BT$ is the inverse temperature. The time step is set to $\Delta t=0.05$. The A and B regions itself are defined as ellipsoidal regions around the minima (x_m,y_m) as $\{x,y|(x-x_m)^2+(1/16)(y-y_m)^2<R^2\}$. The radius is set to $R=0.5$.

2. RETIS using linear interfaces

To obtain a proper RPE for the z-potential we performed TIS simulations. We chose 28 linear interfaces ($n=29$, not counting the stable state definitions λ_0 and λ_n), which are parametrized by $y=ax+\lambda$, with $a=-0.2$. This choice for the slope of the interfaces was determined by trial and error and allows pathways to find their way over the barrier [using just a vertical ($a=\infty$) or horizontal ($a=0$) interface will fail to do so]. The variable λ takes the values $\{-5.5, -5, -4.5, -4.25, -4, -3.75, -3, -1.5, -1, -0.5, 0.5, 0.75, 1, 1.5\}$ for the first 14 interfaces, which are used to sample the AB transition. The other 14 interfaces are used to sample the BA transition and are defined by λ-values $\{-1.5, -1, -0.75, -0.5, 0.5, 1, 1.5, 3, 3.75, 4, 4.25, 4.5, 5, 5.5\}$. All 28 interfaces are depicted in Fig. 2. While we could perform regular TIS, we improve the sampling by applying the replica exchange version of TIS. Following the scheme proposed by van Erp,[17] we include two additional interfaces at -5.5 and 5.5 in order to sample the stable states, to calculate the fluxes ϕ_{01} and $\phi_{n,n-1}$, as well as to achieve much better sampling. In total there are 30 replicas. An AB path created by shooting random trajectories from the origin acted as the initial path for all interfaces. The settings of the dynamics were as above: the time step $\Delta t=0.05$, the friction $\gamma=1$, and the inverse temperature $\beta=4$. We performed 10 000 shooting moves for each interface. In addition, we attempted an equal amount of swaps between neighboring interfaces and an equal amount of time reversals. These latter two types of moves are very cheap, as they do not require integration of the equations of motion. Reversal of paths within an interface is only possible for AA or BB pathways. Attempts to swap interfaces between the two sets of interfaces (for the AB transition and BA transition) were only successful if both paths were connecting the two stable states. During such a swap the paths are time-reversed, i.e., an AB trajectory becomes a BA trajectory and vice versa. The acceptance ratio for the shooting moves ranged between 50% and 80%, due to biasing of the shooting points toward the interface location.[18] The swapping acceptance ratio ranged between 0.1 and 0.8. The reversal ratio was close to unity, except for the replicas belonging to the middle interfaces, as these sampled more AB and BA paths. The wide range of swapping acceptance ratios indicates that the position of the interfaces could be further optimized. The average path length varies from a few hundred time steps for the interfaces close to the stable states to almost 10 000 time steps for the middle replicas. Paths are saved for further analysis every 100th shooting move.

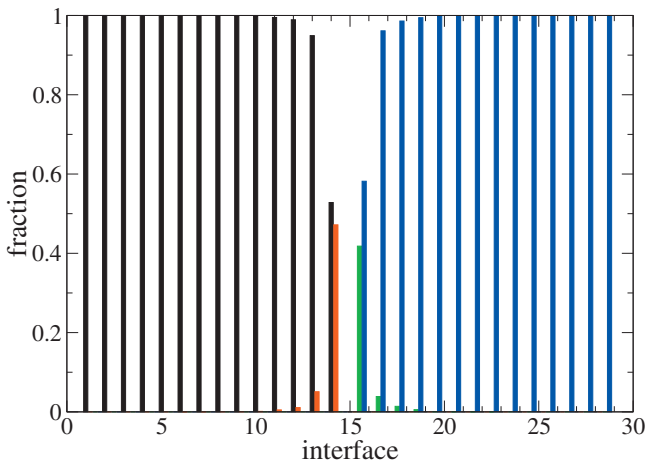

FIG. 3. The fraction of AA, AB, BA, and BB paths for each interface. The color code is black=AA, red=AB, green=BA, and blue=BB. As there are no AA and AB paths for interfaces beyond 14, a gap appears in the plot around interface 15.

Figure 3 shows the fraction of path types occurring in each replica. Only in the middle six replicas there is a substantial fraction of paths connecting both states.

From the path ensembles we construct the crossing probability histograms, which we can join with WHAM (see

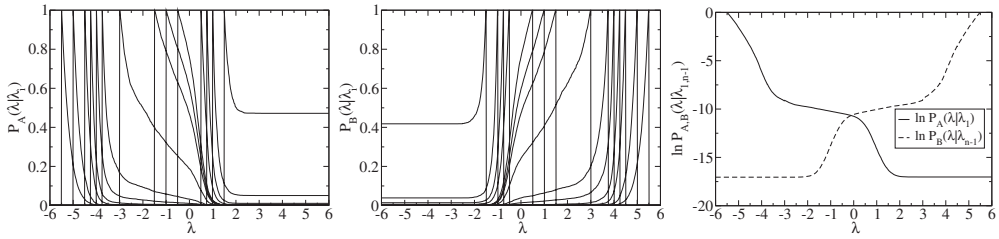

FIG. 4. Crossing probabilities for the TIS simulations employing linear interfaces. The left panel is for the forward transition *AB*, the middle panel for the *BA* transition. The probabilities for interface i start at 1 and then decrease monotonically. The histograms overlap each other, allowing for the application of WHAM. The right panel shows the logarithm of the crossing probabilities $P_A(\lambda|\lambda_1)$ (solid) and $P_B(\lambda|\lambda_{n-1})$ (dashed).

Fig. 4). The final values of the crossing histograms $\ln P_A(\lambda_n|\lambda_1)=-17.03$ and $\ln P_B(\lambda_1|\lambda_n)=-17.04$ are equal, as expected for this symmetric potential. The flux through the first and last interface is $\phi_{01}=1/50.7$ and $\phi_{n,n-1}=1/51.0$, respectively. The corresponding (dimensionless) rate constants are $k_{AB}=7.9\times10^{-10}$ and $k_{BA}=7.8\times10^{-10}$.

3. RETIS using string interfaces

Due to the shape of the z-potential it is rather difficult to obtain a good sampling using linear interfaces and the applied RETIS might thus not be optimal. (Note that this is already much less the case compared to employing, e.g., umbrella sampling due to the nonlocal nature of the shooting move.) As an alternative to imposing linear interfaces the progress parameter λ can also be parametrized by a string description.[27] The string consists of M beads (referred to as images) connecting the minima of the stable states. The original string method optimizes the string to follow the minimum energy path. One of the ingredients of the method is the redistribution of the images along the string such that they are equidistant in the collective variable space[27] (see Fig. 5). During the TIS simulation each configuration along the trajectories is assigned to the nearest images on the string by a Voronoi construction. Linear interpolation yields a continuous value of λ along the string. Alternatively, one can make use of splines, or of other geometrical projection procedures. To remove the influence of different choices of units for the collective variables, one can optimize the string including an additional scaling factor, or one can follow the approach lined out in Ref. 28. Note that a choice of dynamically coupled collective variables might render these projection methods problematic as in that case the isocommittor surfaces are no longer orthogonal to the string.[29,30]

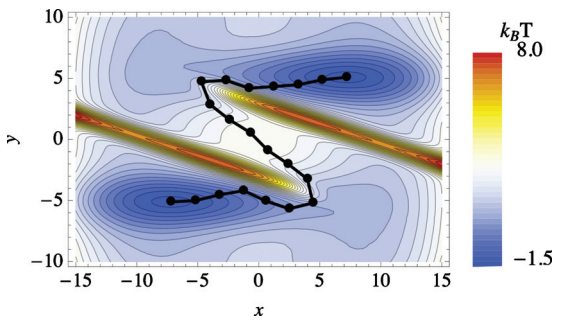

FIG. 5. A string can be employed as a series of interfaces in a TIS simulation. By a Voronoi construction, each point can be assigned to an image on the string. The projections are made continuous by linear interpolation or a geometrical projection method as explained in the appendices.

We used a string with 20 images, obtained from a nonlinear reaction coordinate analysis.[20] Here, the λ value for each configuration along the TIS trajectories was determined by a geometrical projection method as described in Appendix B. This projection returns a continuous $\lambda=\sigma$ value between 0 and 1. As the projection method requires subsequent images to be equidistant also in the collective variable space, we apply the reparametrization scheme of Ref. 27.

The interfaces were again divided in two sets: 14 interfaces for the *AB* transition were placed at $\lambda=\{0.1,0.125,0.15,0.175,0.2,0.25,0.3,0.325,0.35,0.375,0.40,0.425,0.45,0.5\}$, while the 14 interfaces for the *BA* transition were positioned at $\lambda=\{0.5,0.55,0.575,0.6,0.625,0.65,0.7,0.75,0.775,0.8,0.825,0.85,0.875,0.9\}$. These values were chosen such that the exchange between interfaces is roughly equal for most TIS ensembles. In addition, we again included an additional first and last interface at $\lambda=0.1$ and $\lambda=0.9$ in order to enhance the sampling and simultaneously compute the fluxes ϕ_{01} and $\phi_{n,n-1}$.[17] Note that we need only one common interface between the forward and backward transition at $\lambda=0.5$ due to the smaller hysteresis. The acceptance ratios were comparable to those obtained in the TIS simulations utilizing the linear interfaces. Paths were saved for further analysis each 100th shooting move.

Using the same analysis as above, we computed the crossing histograms and applied WHAM. Figure 6 shows the joint crossing probability for both the *AB* and *BA* transitions. The final values of the crossing histograms $\ln P_A(\lambda_n|\lambda_1)=-14.53$ and $\ln P_B(\lambda_1|\lambda_n)=-14.52$ are equal within the error bar. The flux through the first and last interface is $\phi_{01}=1/292.3$ and $\phi_{n,n-1}=1/286.3$, respectively. The corresponding rate constants are $k_{AB}=1.67\times10^{-9}$ and $k_{BA}=1.72\times10^{-9}$. Note that the rate constants are slightly larger than for the linear interfaces, possibly caused by an improved sampling.

4. Projection of the reweighted path ensemble

Using the weights obtained from the RETIS sampling employing the string as an interface progress parameter, we can construct the RPE from Eq. (13). Here, the constants c_A and c_B are identical due to the symmetry of the potential. The free energy in the x-y plane follows from Eq. (15) and is plotted in Fig. 7. The free energy recovers the original z-potential. Indeed the difference between the projected free energy and the original potential is constant within around

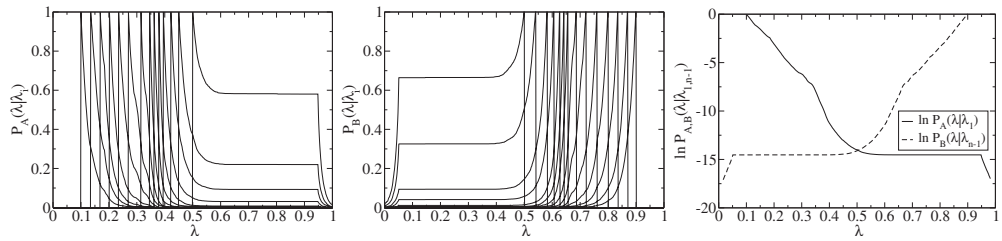

FIG. 6. Crossing probabilities for the TIS simulations using the string interface description. The left panel is for the forward transition *AB* and the middle panel is for the *BA* transition. The probabilities for interface *i* start at 1 and then decrease monotonically. The histograms overlap each other, allowing for application of WHAM. The right panel shows the logarithm of the crossing probabilities $P_A(\lambda|\lambda_1)$ (solid) and $P_B(\lambda|\lambda_{n-1})$ (dashed).

$0.3k_BT$, in the important regions of the *x*-*y* plane. Naturally, this does not include the high potential ridges, which are not sampled in the TIS. The residual difference is possibly caused by the limited number of paths (2800, resulting in 1 351 929 data points) and the large amount of histogram bins (2500).

In addition to the free energy we can project the committor p_B to the *x*-*y* plane. This information is usually unavailable, if we do not have the complete unbiased path ensemble. Using the reweighting scheme of Eq. (16) we plot the committor in Fig. 7. As expected, the committor is close to zero in the stable state *A*. Only when reaching the transition state region [around $(x,y)=(2,-2)$] the committor rises quickly and reaches unity [around $(x,y)=(-2,2)$]. From then on, the committor is almost unity. While these values really are close to zero and unity, the statistics of the RPE still allows an accurate estimate of the committors. This accuracy is useful when trying to optimize the reaction coordinate far away from the transition states.[20]

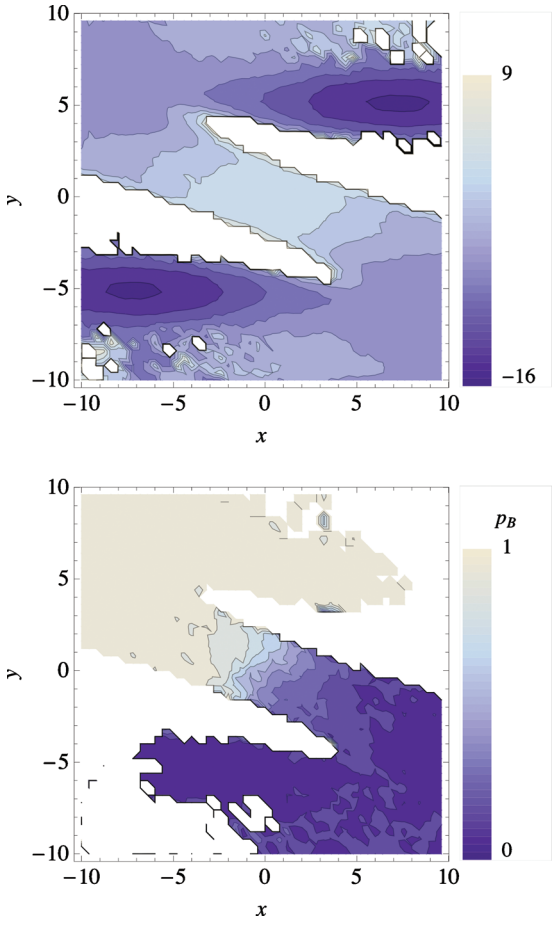

FIG. 7. Top: projected free energy $\beta F=-\log \rho(x,y)$ in the x,y plane recovers the original potential βV, for $\beta=4$. Bottom: projected committor function. The committor is almost zero in the initial state *A*, rises quickly around the transition state region, and becomes unity in the final state *B*.

B. Trp-cage

To illustrate the usefulness of the reweighted path ensemble, we apply it to the TIS simulation results of the Trp-cage mini protein.[22] The Trp-cage is a small protein consisting of 20 residues. In the native folded state it adopts an α-helix (residues 2–8), a 3-helix (residues 11–14) and a polyproline II helix (residues 17–19) (see Fig. 8). The miniprotein folds in a two-state manner from an unfolded to a native state, with a folding rate $k\approx(4.1\ \mu s)^{-1}$.

In previous work we have applied TPS and TIS to the folding/unfolding equilibrium of this protein. We found that there were two possible folding routes. On one route the polypeptide first forms the main secondary structure, the α-helix, followed by the appearance of the tertiary contacts. On the second pathway the tertiary contacts precede the formation of the secondary structure elements. The TPS simulations indicated that the last route was most abundant. For completeness we show this N-L transition in Fig. 8. During the sampling we monitored (among others) the following order parameters: the protein radius of gyration using the α-carbons only (rg), the fraction of native contacts (nc), the root mean square deviation from the native α-carbons structure (rmsd), the root mean square deviation of the α-helical residues 2–8 from an ideal helix (rmsdhx), the solvent acces-

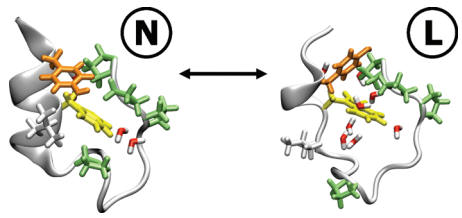

FIG. 8. Initial and final configurations of the rate-limiting transition along the U-L-N folding route, one of the two major folding routes for the Trp-cage. The backbone of the configurations is plotted in white, in cartoon representation. Hydrophobic side-chains forming the tryptophan pocket are plotted in licorice: tryptophan side-chain in yellow, proline amino acids in green, tyrosine in orange, and lysine in white. Water molecules within 3 Å of the side-chain of Trp-6 are plotted in licorice, with oxygen atoms in red and hydrogen in white.

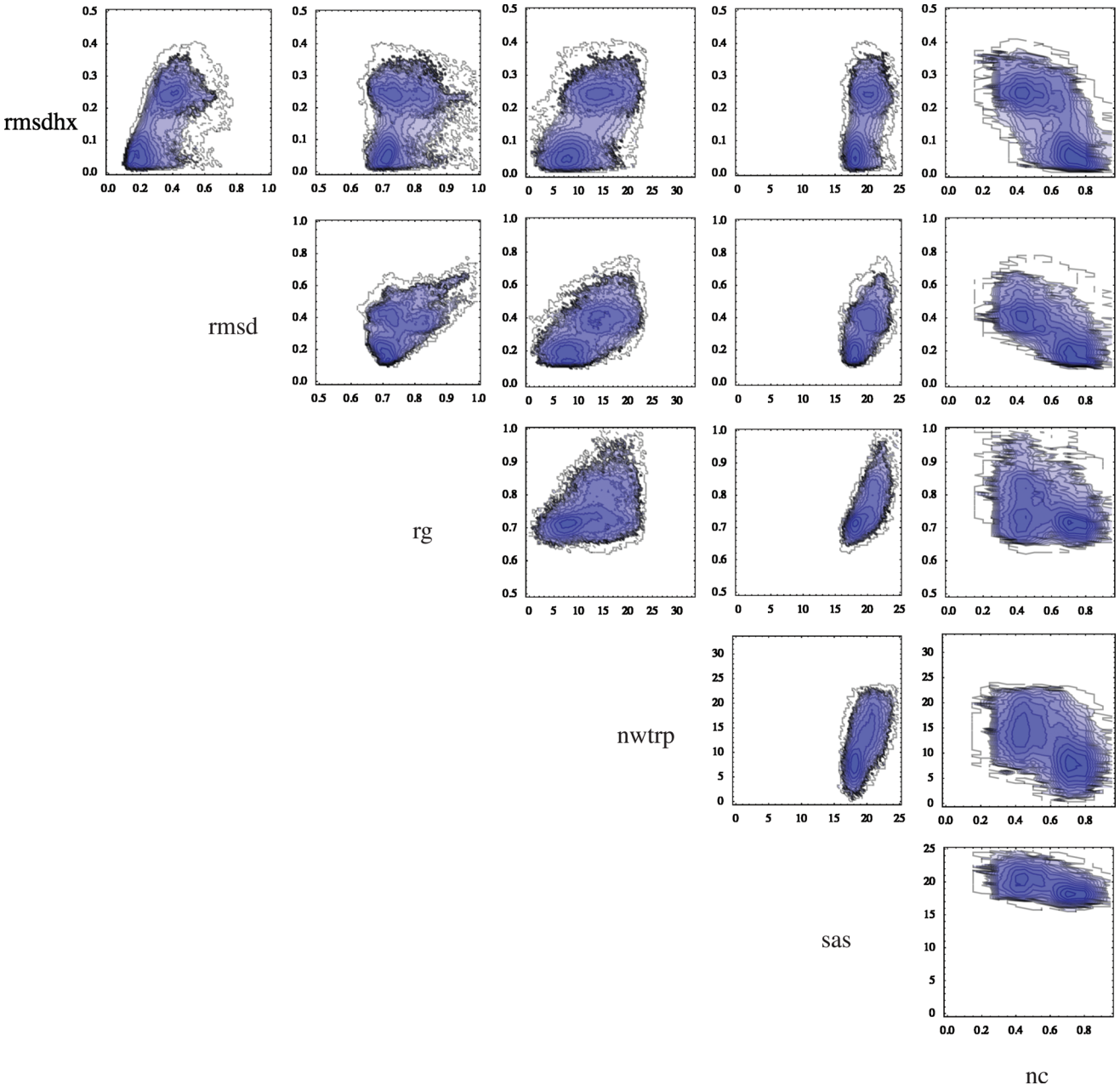

FIG. 9. The free energy profiles of the L-N transition in the Trp-cage system. The contours are separated by $1k_BT$. The profiles are plotted as a function of all possible combinations of pairs of the monitored collective variables. They are ordered in a grid, such that both the x axis and the y axis of both rows and columns of plots are identical. The labels simultaneously refer to the x axis above it and the y axis to the right.

sible surface (sas) of the whole protein, and the number of water molecules around tryptophan (nwtrp). We computed the rate constants for the rate-limiting step on the first route using TIS, with the rmsdhx as the interface defining variable. In addition, we performed a likelihood maximization analysis[25] and found that a combination of the rmsdhx and rmsd described the reaction best. In Refs. 21 and 22 we reported on the mechanism, the kinetic rate constants, and the reaction coordinate, but did not discuss the free energy profile. With the current methodology it is possible to extract the free energy and the committor surfaces as a function of arbitrary projections. To do so, the TIS path ensembles are reweighted using the same WHAM weights as reported in Ref. 22. The constants c_A and c_B in Eq. (12) are obtained from the rate constants reported in Ref. 22. Subsequently, the paths can be projected on any set of collective variables using Eq. (15) in order to obtain the free energy. In Fig. 9 we plot the free energy landscapes as a function of pairs of collective variables. In this way we have access to a six dimensional free energy landscape. Note that while many free energy landscapes exhibit two minima, some only have a single one. The projection enables additional insights, such as that the z-shaped free energy landscape in the nc, rmsdhx plane indicates that the rmsdhx collective variable changes independently of the number of native contacts nc. Also, in the rg, rmsd plane, a third state seems to be visited at higher radius of gyration during the transition. Note that these features did not stand out from the path ensembles in Refs. 21 and 22. Hence, the RPE projection enables new insight in the mechanism of the Trp-cage N-L transition.

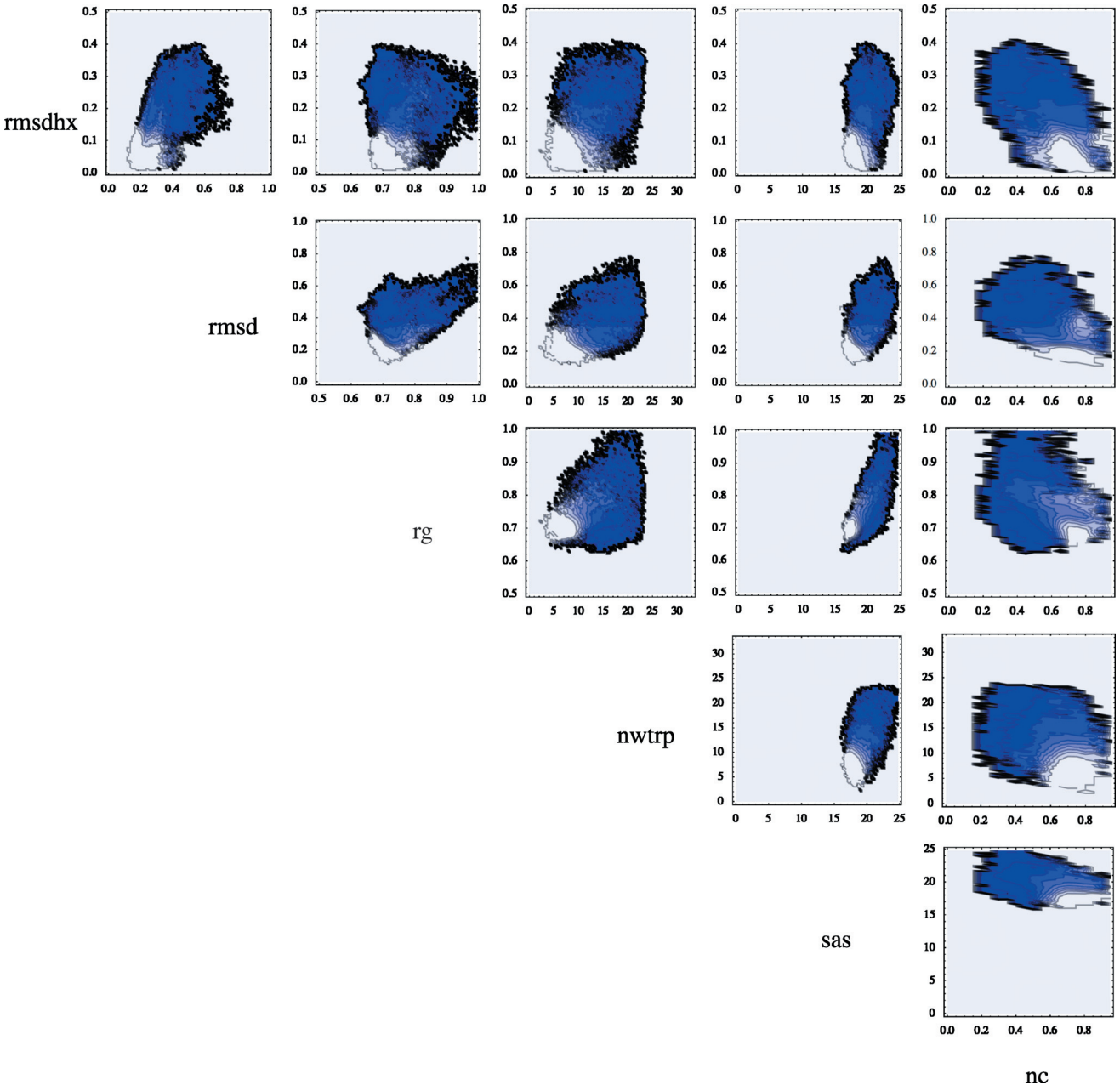

FIG. 10. The averaged committor $\bar{p}_B$ of the L-N transition in the Trp-cage system. White is $\bar{p}_B=0$ and blue denotes $\bar{p}_B=1$. The grid of plots is organized as in Fig. 9.

In Fig. 10 we plot the committor functions in the same landscapes. From these figures, the transition state region can be immediately deduced, and interestingly does not always correspond to the free energy saddle point. Moreover, in several projections, e.g., nwtrp,rg, the $p_B=0.5$ surface is clearly nonlinear. Analysis of the committor surfaces gives unprecedented insight in the reaction coordinate (see also Ref. 20).

IV. CONCLUSION

We have introduced a reweighting procedure for path sampling that allows to join the path ensembles in a TIS simulation series into one single large reweighted path ensemble that has the same properties as the unbiased path ensemble. The main difference is that the rare pathways that very seldom occur in an unbiased ensemble now are much more abundant due to the bias that the path sampling introduces. The reweighting scheme corrects for this bias. The gain is that we have access to accurate statistics over the entire path space between the two stable states. In addition, the reweighting scheme allows for the projection of the path ensemble on arbitrary collective variables. This is useful if one wants to study free energy profiles in many different landscapes besides the imposed TIS progress parameter. The importance of the reweighting scheme is further emphasized by the fact that the free energy landscape is generally not available from path sampling. Also the (averaged) committor function is available due to the knowledge of the destination of each path in the ensemble. Moreover, the RPE allows, unlike free energy biasing schemes, to investigate the order of events, as registered by collective variables. We note that

the RPE is also available in the FFS method,[14] because there the path probabilities are automatically reweighted at each interface. However, because the backward paths are not sampled in FFS, it has different convergence properties.

The RPE can also help identifying complex nonlinear reaction coordinates that span the entire mechanism from initial state to final state. This will be the subject of another paper in this volume.[20]

ACKNOWLEDGMENTS

This work was financially supported by the "Nederlandse Organisatie voor Wetenschappelijk Onderzoek (NWO)" and the "Stichting Nationale Computerfaciliteiten" (NCF).

APPENDIX A: THE REWEIGHTED PATH ENSEMBLE

In this appendix we show that the RPE expression Eq. (11) is equivalent to the unbiased paths ensemble Eq. (10) for paths leaving stable state A. In the TIS framework the path probability of interface i reads

$$\mathcal{P}_{A\Lambda_i}[\mathbf{x}^L] = \tilde{h}_i[\mathbf{x}^L]\pi[\mathbf{x}^L]/Z_{A\Lambda_i}, \tag{A1}$$

with again $Z_{A\Lambda_i}$ as the normalizing factor

$$Z_{A\Lambda_i} \equiv \int \mathcal{D}\mathbf{x}\tilde{h}_i[\mathbf{x}^L]\pi[\mathbf{x}^L], \tag{A2}$$

where $\tilde{h}_i[\mathbf{x}^L]$ is given in Eq. (7) and $\Lambda_i^+ = \{\mathbf{x}:\lambda(\mathbf{x}) > \lambda_i\}$. The reweighted path ensemble (from A) is defined as the sum of the path ensembles over the interfaces, where each interface is weighted properly. To derive how the interfaces are weighted, we first look at how the crossing probability is weighted using WHAM.

The crossing histograms are constructed by monitoring the maximum λ-value along a path in the ensemble using a θ-function:

$$P_A(\lambda|\lambda_i) = \int \mathcal{D}\mathbf{x}\mathcal{P}_{A\Lambda_i}[\mathbf{x}^L]\theta(\lambda_{\max}[\mathbf{x}^L] - \lambda), \tag{A3}$$

where $\lambda_{\max}[\mathbf{x}^L]$ is the maximum value of λ reached for each trajectory $\mathbf{x}^L$ in the path ensemble $A\Lambda_i$ and θ is the Heaviside step function. The total histogram is constructed from the TIS ensembles for interface $i = 1 \cdots n-1$ (Ref. 31) by applying the WHAM (multiple histogram method),[16]

$$P_A(\lambda|\lambda_1) = \sum_{i=1}^{n-1} \bar{w}_i^A \theta(\lambda_{i+1} - \lambda)\theta(\lambda - \lambda_i) \sum_{j=1}^{i} P_A(\lambda|\lambda_j). \tag{A4}$$

The weights $\bar{w}_i^A$ are given by

$$\bar{w}_i^A = \frac{1}{\Sigma_{j=1}^{i} 1/w_j^A}, \tag{A5}$$

where w_j^A are the optimized WHAM weights for each interface histogram. Note that the λ_0 and λ_n interfaces are excluded from these sums, as they (usually) denote the stable state definitions themselves. Defining the function

$$\theta_i(\lambda) = \theta(\lambda_{i+1} - \lambda)\theta(\lambda - \lambda_i), \tag{A6}$$

and combining Eqs. (A1), (A3), and (A4) the reweighted histogram becomes

$$\begin{aligned} P_A(\lambda|\lambda_1) &= \sum_{i=1}^{n-1} \bar{w}_i^A \theta_i(\lambda) \sum_{j=1}^{i} \int \mathcal{D}\mathbf{x}\mathcal{P}_{A\Lambda_j}[\mathbf{x}^L]\theta(\lambda_{\max}[\mathbf{x}^L] - \lambda) \\ &= \sum_{i=1}^{n-1} \bar{w}_i^A \theta_i(\lambda) \sum_{j=1}^{i} \int \mathcal{D}\mathbf{x}\frac{\tilde{h}_j[\mathbf{x}^L]\pi[\mathbf{x}^L]}{Z_{A\Lambda_j}}\theta(\lambda_{\max}[\mathbf{x}^L] - \lambda) \\ &= \int \mathcal{D}\mathbf{x}\left(\sum_{i=1}^{n-1} \bar{w}_i^A \theta_i(\lambda) \sum_{j=1}^{i} \frac{\tilde{h}_j[\mathbf{x}^L]}{Z_{A\Lambda_j}}\right)\pi[\mathbf{x}^L]\theta(\lambda_{\max}[\mathbf{x}^L] - \lambda). \end{aligned} \tag{A7}$$

This reweighted histogram should be clearly the same as the histogram based on paths only restricted to start in A.

$$\begin{aligned} P_A(\lambda|\lambda_1) &= \int \mathcal{D}\mathbf{x}\mathcal{P}_A[\mathbf{x}^L]\theta(\lambda_{\max}[\mathbf{x}^L] - \lambda) \\ &= \int \mathcal{D}\mathbf{x}\frac{h_A(\mathbf{x}_0)}{Z_A}\pi[\mathbf{x}^L]\theta(\lambda_{\max}[\mathbf{x}^L] - \lambda), \end{aligned} \tag{A8}$$

with

$$Z_A \equiv \int \mathcal{D}\mathbf{x}h_A(\mathbf{x}_0)\pi[\mathbf{x}^L]. \tag{A9}$$

Equation (A4) can be only equal to Eq. (A8) if for each path $\mathbf{x}^L$

$$\sum_{i=1}^{n-1} \bar{w}_i^A \theta_i(\lambda) \sum_{j=1}^{i} \frac{\tilde{h}_j[\mathbf{x}^L]}{Z_{A\Lambda_j}} = \frac{h_A(\mathbf{x}_0)}{Z_A}. \tag{A10}$$

For each path in the ensemble of the ith interface $h_A(\mathbf{x}_0) = 1$, and $\tilde{h}_j[\mathbf{x}^L] = 1$ for $j \leq i$, and thus

$$\sum_{i=1}^{n-1} \bar{w}_i^A \theta_i(\lambda) \sum_{j=1}^{i} \frac{1}{Z_{A\Lambda_j}} = \frac{1}{Z_A}. \tag{A11}$$

This equation can only hold for each λ if for each i

$$\bar{w}_i^A = 1/\sum_{j=1}^{i} \frac{Z_A}{Z_{A\Lambda_j}}. \tag{A12}$$

This is indeed the WHAM solution (A5), with $w_j^A = Z_{A\Lambda_j}/Z_A$.[4,16]

In the same way as the crossing histograms we can reweight the paths in the TIS path ensemble. By defining the function $g[\mathbf{x}^L]$

$$g_i^A[\mathbf{x}^L] = \theta(\lambda_{\max}[\mathbf{x}^L] - \lambda_i)\theta(\lambda_{i+1} - \lambda_{\max}[\mathbf{x}^L]), \tag{A13}$$

we can select only those paths that reach their maximum λ between interface i and $i+1$. First, we use the function $g_i[\mathbf{x}^L]$ to select the paths for interface i. Then the total path ensemble is constructed from the crossing histogram weights using a similar reweighting scheme as in WHAM:

$$\mathcal{P}_A[\mathbf{x}^L] = \sum_{i=1}^{n-1} \bar{w}_i' g_i^A[\mathbf{x}^L] \sum_{j=1}^{i} \mathcal{P}_{A\Lambda_j}[\mathbf{x}^L]$$
$$= \sum_{i=1}^{n-1} \bar{w}_i' g_i^A[\mathbf{x}^L] \sum_{j=1}^{i} \frac{\tilde{h}_j^A[\mathbf{x}^L]}{Z_{A\Lambda_j}} \pi[\mathbf{x}^L]$$
$$= \left(\sum_{i=1}^{n-1} \bar{w}_i' g_i^A[\mathbf{x}^L] \sum_{j=1}^{i} \frac{\tilde{h}_j^A[\mathbf{x}^L]}{Z_{A\Lambda_j}} \right) \pi[\mathbf{x}^L], \tag{A14}$$

where $\bar{w}_i'$ is the weighting factor for interface i, with $0<i<n$. The reweighted path ensemble must naturally be the same as the unconditional path ensemble to leave A,

$$\mathcal{P}_A[\mathbf{x}^L] = h_A(\mathbf{x}_0)\pi[\mathbf{x}^L]/Z_A. \tag{A15}$$

Again, Eq. (A14) can only be equal to Eq. (A15) for all possible paths when the following holds for each path $\mathbf{x}^L$:

$$\sum_{i=1}^{n-1} \bar{w}_i' g_i^A[\mathbf{x}^L] \sum_{j=1}^{i} \frac{\tilde{h}_j^A[\mathbf{x}^L]}{Z_{A\Lambda_j}} = \frac{h_A[\mathbf{x}_0]}{Z_A}. \tag{A16}$$

For each path in the ensemble of interface i the function $\tilde{h}_j[\mathbf{x}^L]=1$ for $j \le i$, and thus

$$\sum_{i=1}^{n-1} \bar{w}_i' g_i^A[\mathbf{x}^L] \sum_{j=1}^{i} \frac{1}{Z_{A\Lambda_j}} = \frac{1}{Z_A}, \tag{A17}$$

because each path (I) belongs to an interface i, (II) when belonging to interface i it also belongs to each previous interface, and (III) each path starts in A. It follows that the above condition (A17) can only be fulfilled if for each interface,

$$\bar{w}_i' = 1/\sum_{j=1}^{i} \frac{Z_A}{Z_{A\Lambda_j}}. \tag{A18}$$

Comparing the above equation with Eq. (A12) leads to the conclusion that $\bar{w}_j' = \bar{w}_j^A$, and hence that the WHAM weights for the crossing histograms are the same as for the RPE,

$$w_j' = w_j^A = Z_{A\Lambda_j}/Z_A. \tag{A19}$$

In other words, by identifying the crossing probability weights using WHAM we obtained the path weights.

Expression (A14) for the reweighted path ensemble $\mathcal{P}_A[\mathbf{x}^L]$ can be simplified by rearranging the order of the sums.

$$\mathcal{P}_A[\mathbf{x}^L] = \sum_{i=1}^{n-1} \bar{w}_i' g_i^A[\mathbf{x}^L] \sum_{j=1}^{i} \frac{\tilde{h}_j^A[\mathbf{x}^L]}{Z_{A\Lambda_j}} \pi[\mathbf{x}^L]$$
$$= \sum_{j=1}^{n-1} \frac{\tilde{h}_j^A[\mathbf{x}^L]}{Z_{A\Lambda_j}} \sum_{i=1}^{n-1} \bar{w}_i^A g_i[\mathbf{x}^L] \pi[\mathbf{x}^L]. \tag{A20}$$

This is allowed because the sum over $j=1$ to i can be extended to $j=1$ to n, because $\tilde{h}_j^A[\mathbf{x}^L]=0$ for $j>i$ due to the selection by $g_i[\mathbf{x}^L]$. By defining a path weight $W^A[\mathbf{x}^L] \equiv \Sigma_{i=1}^{n-1} \bar{w}_i^A g_i^A[\mathbf{x}^L]$ for each path $\mathbf{x}^L$ in the ensemble, the expression for the probability for paths leaving A becomes

$$\mathcal{P}_A[\mathbf{x}^L] = \sum_{j=1}^{n-1} \frac{\tilde{h}_j^A[\mathbf{x}^L]}{Z_{A\Lambda_j}} W^A[\mathbf{x}^L] \pi[\mathbf{x}^L], \tag{A21}$$

$$= \sum_{j=1}^{n-1} \mathcal{P}_{A\Lambda_j}[\mathbf{x}^L] W^A[\mathbf{x}^L]. \tag{A22}$$

The latter equality is identical to Eq. (11) in the main text.

The forward and reverse reweighted path ensembles need to be combined to retrieve the complete RPE. Defining the indicator function

$$\tilde{h}_i^B[\mathbf{x}^L] = \begin{cases} 1 & \text{if } \mathbf{x}_0 \in B \wedge \mathbf{x}_L \in (A \cup B) \wedge \\ & \forall \{j | 0 < j < L\}: \mathbf{x}_j \notin (A \cup B) \wedge \\ & \exists \{j | 0 < j < L\}: \mathbf{x}_j \in \Lambda_i^- \\ 0 & \text{otherwise,} \end{cases} \tag{A23}$$

with $\Lambda_i^- = \{\mathbf{x}: \lambda(\mathbf{x}) < \lambda_i\}$, we can write the path probability for the reverse process $B \to A$ in a similar expression as for $\mathcal{P}_A[\mathbf{x}^L]$,

$$\mathcal{P}_B[\mathbf{x}^L] = \sum_{j=1}^{n-1} \mathcal{P}_{B\Lambda_j}[\mathbf{x}^L] W^B[\mathbf{x}^L], \tag{A24}$$

$$= \sum_{j=1}^{n-1} \frac{\tilde{h}_j^B[\mathbf{x}^L]}{Z_{B\Lambda_j}} W^B[\mathbf{x}^L] \pi[\mathbf{x}^L], \tag{A25}$$

with the path weight $W^B[\mathbf{x}^L] \equiv \Sigma_{i=1}^{n-1} \bar{w}_i^B g_i^B[\mathbf{x}^L]$ where $\bar{w}_i^B = (\Sigma_{j=1}^{i} Z_B / Z_{B\Lambda_j})^{-1}$ are the interface WHAM weights for the reverse process. Z_B and $Z_{B\Lambda_j}$ are defined in a similar way as Eqs. (A9) and (A2), respectively. The path selection function $g_i^B[\mathbf{x}^L]$ is

$$g_i^B[\mathbf{x}^L] = \theta(\lambda_{\min}[\mathbf{x}^L] - \lambda_i)\theta(\lambda_{i-1} - \lambda_{\min}[\mathbf{x}^L]), \tag{A26}$$

where $\lambda_{\min}[\mathbf{x}^L]$ is now the *minimum* value of λ reached along the trajectory $\mathbf{x}^L$.

For the complete RPE we need to combine the two ensembles

$$\mathcal{P}[\mathbf{x}^L] = c_A \mathcal{P}_A[\mathbf{x}^L] + c_B \mathcal{P}_B[\mathbf{x}^L]. \tag{A27}$$

Using two independent (forward and reverse) TIS simulations series the unknown constants c_A and c_B can be computed by matching the boundary and loop histograms as was done for the free energy.[15] We define the functions

$$p(\lambda) = \int \mathcal{D}\mathbf{x} \sum_{k=0}^{L} \delta(\lambda(\mathbf{x}_k) - \lambda) \mathcal{P}[\mathbf{x}^L], \tag{A28}$$

$$p_A(\lambda) = \int \mathcal{D}\mathbf{x} \sum_{k=0}^{L} \delta(\lambda(\mathbf{x}_k) - \lambda) \mathcal{P}_A[\mathbf{x}^L], \tag{A29}$$

$$p_B(\lambda) = \int \mathcal{D}\mathbf{x} \sum_{k=0}^{L} \delta(\lambda(\mathbf{x}_k) - \lambda) \mathcal{P}_B[\mathbf{x}^L], \tag{A30}$$

where the last function $p_B(\lambda)$ should not be confused with the committor. Then the probability to find the system at a value of λ is

$$p(\lambda) = c_A p_A(\lambda) + c_B p_B(\lambda). \tag{A31}$$

In order to obtain the constants c_A and c_B we can match the boundary histograms at a certain interface i, as was done for the free energy in Ref. 15,

$$p(\lambda) \propto s_{AB}(\lambda_i)\frac{p_A(\lambda)}{p_A(\lambda_i)} + s_{BA}(\lambda_i)\frac{p_B(\lambda)}{p_B(\lambda_i)}. \tag{A32}$$

The scaling factor is $s_{AB}=m_{Ai}(\lambda_i)/m_{AB,i}(\lambda_i)$, where $m_{Ai}(\lambda_i)$ is the un-normalized and unmatched p_{Ai} histogram for the region λ_i to λ_{i+1}, and $m_{AB,i}(\lambda_i)$ is the un-normalized and unmatched histogram for AB paths only for the same region. Similarly, $s_{BA}=m_{Bi}(\lambda_i)/m_{BA,i}(\lambda_i)$, with $m_{Bi}(\lambda_i)$ as the un-normalized and unmatched p_{Bi} histogram for the region λ_{i-1} to λ_i, and $m_{BA,i}(\lambda_i)$ the BA histograms for the same region. In short, this rescaling matches the AB histograms with the BA histograms for each region, as they should be exactly the same by definition (the BA and AB histograms were called the boundary histograms in Ref. 15). Having matched the histograms, constants c_A and c_B are

$$c_A = \frac{s_{AB}(\lambda_i)}{p_A(\lambda_i)}, \quad c_B = \frac{s_{BA}(\lambda_i)}{p_B(\lambda_i)}, \tag{A33}$$

for each interface i. If the flux and the crossing probabilities are known, one can also use the resulting rate constants to compute the constants c_A and c_B.[18]

Summarizing, when a complete TIS simulation is done, one ends up with path ensembles of n interfaces for both the $A\to B$ and $B\to A$ directions. After matching the crossing probabilities one obtains the weights w_i and fitting the free energy gives c_A and c_B. The expression for the RPE based on these simulations is then

$$\mathcal{P}[\mathbf{x}^L] = c_A \sum_{j=1}^{n-1} \mathcal{P}_{A\Lambda_j}[\mathbf{x}^L] W^A[\mathbf{x}^L], \tag{A34}$$

$$+ c_B \sum_{j=1}^{n-1} \mathcal{P}_{B\Lambda_j}[\mathbf{x}^L] W^B[\mathbf{x}^L], \tag{A35}$$

which is identical to Eq. (12).

As is explained in the main text, the contributions $P^-_{\lambda_1}$ and $P^+_{\lambda_{n-1}}$ need to be added to obtain the complete path ensemble $\mathcal{P}_c[\mathbf{x}^L]$. Using the RETIS approach[17,18] all contributions to the RPE can be sampled simultaneously and efficiently.

APPENDIX B: GEOMETRICAL PROJECTION ONTO THE STRING

In the space spanned by the collective variables that are used to define a transition pathway as a string of N equidistant images positioned at $\{\mathbf{s}_1, \mathbf{s}_2, \ldots, \mathbf{s}_N\}$, an arbitrary point $\mathbf{p}$ can be projected on that string in a smooth manner by considering the triplet of closest string images and drawing a circle through them. This is illustrated in Fig. 11 for a point $\mathbf{p}$ that is closest to image i. Image $i-1$ is second closest to $\mathbf{p}$ and image $i+1$ is third closest, defining the circle with midpoint $\mathbf{m}$. To project $\mathbf{p}$ onto the string we take the point where the radian from $\mathbf{m}$ that goes through $\mathbf{p}$ meets the string line piece between $\mathbf{s}_i$ and $\mathbf{s}_{i-1}$. To setup a foliation of the space in the neighborhood of the string and define a continuous progress coordinate σ along the string, we realize that all points closest to $\mathbf{s}_i$ are found in the pie-shaped space bound at the left by the radian from $\mathbf{m}$ that crosses line piece $\mathbf{s}_i - \mathbf{s}_{i-1}$ in the middle (denoted $-1/2$ in Fig. 11) and at the right by the radian that crosses line piece between $\mathbf{s}_{i+1} - \mathbf{s}_i$ in the middle (denoted $+1/2$).

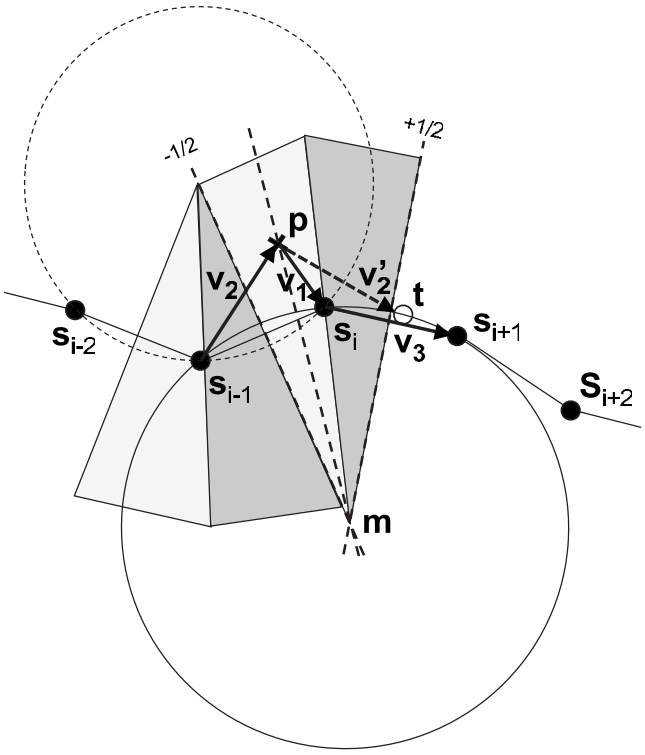

FIG. 11. Smooth foliation of collective variable space in the neighborhood of a parametrized string of images based on the circles that connect each triplet of images.

In the local pie-shaped space, a local progress coordinate ς moves from $-1/2$ to $+1/2$ (in length units of image separation) passing 0 at the radian through $\mathbf{s}_i$. Note that a point $\mathbf{p}$ at $\varsigma=-1/2$ is equidistant to images $i-1$ and i, while at $\varsigma=0$ such a point is equidistant to image $i-1$ and $i+1$. For values in between, there is a point $\mathbf{t}$ on the circle between $\mathbf{s}_i$ and $\mathbf{s}_{i+1}$ for which the distance to $\mathbf{p}$ is equal to the distance between $\mathbf{p}$ and $\mathbf{s}_{i-1}$.

$$|\mathbf{v}_2'| = |\mathbf{t}-\mathbf{p}| \equiv |\mathbf{v}_2| = |\mathbf{p}-\mathbf{s}_{i-1}|. \tag{B1}$$

In Fig. 11, point $\mathbf{t}$ is denoted with an open circle and the vector $\mathbf{v}_2'$ between $\mathbf{t}$ and $\mathbf{p}$ is indicated with a dashed arrow. The fraction of the arc length from $\mathbf{s}_i$ to $\mathbf{t}$ on the circle with respect to that from $\mathbf{s}_i$ to $\mathbf{s}_{i+1}$ is directly related to the value of the progress coordinate: specifically, as this fraction goes from 0 to 1 (i.e., point $\mathbf{t}$ moves from $\mathbf{s}_i$ to $\mathbf{s}_{i+1}$), ς goes from $-1/2$ to 0. Rather than computing arc lengths, we approximate this fraction by considering point $\mathbf{t}'$ that is also equidistant from $\mathbf{p}$ but lies on the straight line piece between $\mathbf{s}_i$ and $\mathbf{s}_{i+1}$ instead of on the curve. The (approximate) fraction f is then

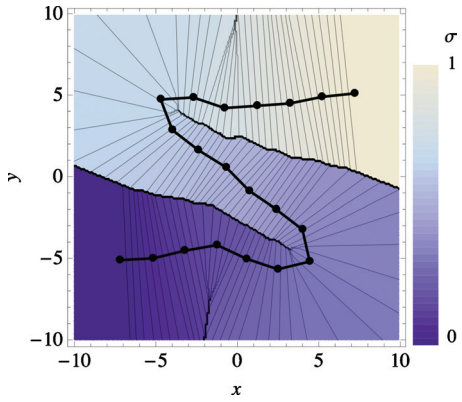

FIG. 12. Continuous projection of points in phase space on a string. The color indicates the value between 0 (purple) and 1 (gray) along the string.

$$f = \frac{|\mathbf{t}' - \mathbf{s}_i|}{|\mathbf{s}_{i+1} - \mathbf{s}_i|}. \tag{B2}$$

Determining $\sigma(\mathbf{p})$ thus requires finding point $\mathbf{t}'$ and fraction f. Using Eqs. (B1) and (B2), we can write

$$|\mathbf{v}_2| = |\mathbf{v}_2'| = |\mathbf{t}' - \mathbf{p}| = |f \cdot (\mathbf{s}_{i+1} - \mathbf{s}_i) + \mathbf{s}_i - \mathbf{p}|,$$
$$|\mathbf{v}_2| = |f \cdot \mathbf{v}_3 + \mathbf{v}_1|, \tag{B3}$$

where we defined the vectors $\mathbf{v}_1 \equiv \mathbf{s}_i - \mathbf{p}$, $\mathbf{v}_2 \equiv \mathbf{p} - \mathbf{s}_{i-1}$, and $\mathbf{v}_3 \equiv \mathbf{s}_{i+1} - \mathbf{s}_i$, as indicated in the figure. Equation (B3) is solved for f using the quadratic formula. The positive root (divided by 2) gives our measure of ς between $-1/2$ and 0, or, in the case that $\mathbf{s}_{i+1}$ was the second closest image to $\mathbf{p}$ and $\mathbf{s}_{i-1}$ the third closest image, it gives the measure between $\varsigma = 0$ and $\varsigma = +1/2$. Therefore, depending on whether $\mathbf{p}$ lies left or right from $\mathbf{s}_i$, $f/2$ is added or subtracted to the string image index i and divided by the number of images N to obtain a smooth progress coordinate between zero and one along the entire string:

$$\sigma = N^{-1}\left(i_{\min} \pm \frac{\sqrt{v_{13}^2 - v_{33}(v_{11} - v_{22})} - v_{13}}{2(v_{33} - 1)}\right), \tag{B4}$$

where $v_{ij} = \mathbf{v}_i \cdot \mathbf{v}_j$. Note that this projection of a phase space point onto a string of equidistant images only requires knowledge of the three closest images and not of the circle center $\mathbf{m}$, so that the application of the projection is also trivial in higher dimensions. In Fig. 12 the foliation is shown for the s-shaped string in our model potential.

[1] G. M. Torrie and J. P. Valleau, Chem. Phys. Lett. **28**, 578 (1974).
[2] H. Grubmüller, Phys. Rev. E **52**, 2893 (1995).
[3] A. Laio and M. Parrinello, Proc. Natl. Acad. Sci. U.S.A. **99**, 12562 (2002).
[4] D. Frenkel and B. Smit, *Understanding Molecular Simulation*, 2nd ed. (Academic, San Diego, CA, 2002).
[5] C. H. Bennett, in *Algorithms for Chemical Computations*, ACS Symposium Series Vol. 46, edited by R. Christofferson (American Chemical Society, Washington, D.C., 1977).
[6] D. Chandler, J. Chem. Phys. **68**, 2959 (1978).
[7] A. F. Voter, J. Chem. Phys. **106**, 4665 (1997).
[8] A. F. Voter, Phys. Rev. Lett. **78**, 3908 (1997).
[9] M. R. Sørensen and A. F. Voter, J. Chem. Phys. **112**, 9599 (2000).
[10] A. F. Voter, Phys. Rev. B **57**, R13985 (1998).
[11] C. Dellago, P. G. Bolhuis, and P. L. Geissler, Adv. Chem. Phys. **123**, 1 (2002).
[12] C. Dellago, P. G. Bolhuis, F. S. Csajka, and D. Chandler, J. Chem. Phys. **108**, 1964 (1998).
[13] T. S. van Erp, D. Moroni, and P. G. Bolhuis, J. Chem. Phys. **118**, 7762 (2003).
[14] R. J. Allen, D. Frenkel, and P. R. ten Wolde, J. Chem. Phys. **124**, 024102 (2006).
[15] D. Moroni, T. S. van Erp, and P. G. Bolhuis, Phys. Rev. E **71**, 056709 (2005).
[16] A. M. Ferrenberg and R. H. Swendsen, Phys. Rev. Lett. **63**, 1195 (1989).
[17] T. S. van Erp, Phys. Rev. Lett. **98**, 268301 (2007).
[18] P. G. Bolhuis, J. Chem. Phys. **129**, 114108 (2008).
[19] D. Minh and J. Chodera, J. Chem. Phys. **131**, 134110 (2009).
[20] W. Lechner, J. Rogal, J. Juraszek, B. Ensing, and P. Bolhuis, J. Chem. Phys. **133**, 174110 (2010).
[21] J. Juraszek and P. G. Bolhuis, Proc. Natl. Acad. Sci. U.S.A. **103**, 15859 (2006).
[22] J. Juraszek and P. G. Bolhuis, Biophys. J. **95**, 4246 (2008).
[23] These Markovian probability distributions depend on the dynamics. For instance, they are delta functions for Hamiltonian dynamics. For the Langevin dynamics employed in this paper they are given by bivariate Gaussian expressions (Ref. 12).
[24] P. G. Bolhuis, C. Dellago, and D. Chandler, Proc. Natl. Acad. Sci. U.S.A. **97**, 5877 (2000).
[25] B. Peters and B. L. Trout, J. Chem. Phys. **125**, 054108 (2006).
[26] B. Peters, G. T. Beckham, and B. L. Trout, J. Chem. Phys. **127**, 034109 (2007).
[27] W. E, W. Ren, and E. Vanden-Eijnden, Phys. Rev. B **66**, 052301 (2002).
[28] E. Vanden-Eijnden and M. Venturoli, J. Chem. Phys. **130**, 194103 (2009).
[29] J. Langer, Ann. Phys. **54**, 258 (1969).
[30] A. Berezhkovskii and A. Szabo, J. Chem. Phys. **122**, 014503 (2005).
[31] Note that λ_0 usually defines the boundary of stable state A, likewise λ_n defines B. Often $\lambda_0 = \lambda_1$ and $\lambda_{n-1} = \lambda_n$, but this is not required, and in fact not the case in this work. See Ref. 32.
[32] T. S. van Erp and P. G. Bolhuis, J. Comput. Phys. **205**, 157 (2005).